NAMT
92-034

Shape Evolution of an Initially Circular Precipitate Growing by Diffusion in an Applied Stress Field

Perry H. Leo
University of Minnesota
Herng-Jeng Jou
University of Minnesota

Research Report No. 92-NA-034

October 1992

Shape evolution of an initially circular precipitate growing by diffusion in an applied stress field

Perry H. Leo [1] and Herng-Jeng Jou [2]

Abstract

The diffusional growth of a precipitate transforming under applied stress is analyzed to determine the shape evolution of the precipitate. The analysis is based on linearizing the precipitate shape about a circle. Because of applied stresses, a circle is a stable shape only when the shear moduli of the precipitate and the surrounding matrix are identical. Otherwise, one finds a non–circular base shape that depends on the applied stress and the elastic constants of both phases. For small precipitate sizes, the progression of growing base shapes are not self–similar, but define a path of fastest growing shapes. The base shapes become unstable at a critical radius that depends on the elastic fields. In particular, the critical radius can be affected by elastic fields even when the shear moduli of the precipitate and matrix are equal.

[1] Assistant Professor, and
[2] Graduate Student, Department of Aerospace Engineering and Mechanics, University of Minnesota, Minneapolis, Minnesota 55455

1 Introduction

It has been well established that the equilibria and kinetics of phase transformations in crystalline alloys can be strongly influenced by elastic energies. Elastic energies may arise from both misfit between phases and applied loads. The importance of elastic effects during phase transitions has been experimentally documented by both adjusting the misfit via small composition changes [1, 2] and by applying stresses during the transformation process [3, 4]. These experiments indicate that stresses have a strong effect on the observed precipitate shapes and alignments on the stresses in the system, though the exact nature of this relationship may be quite complicated.

There has been, in addition to this experimental work, a great deal of theoretical modelling of the role of elasticity in phase transformations and microstructural development. Roughly speaking, this work has followed two approaches. One approach is to consider how the combination of elastic energy and surface energy sets the equilibrium state of the transformed alloy. Many authors have taken this view to study the equilibrium shapes of precipitates that result from both diffusional and martensitic transformations [5-9]. The second approach considers the influence of elasticity on the kinetic evolution of the microstructure by focussing on the interaction between elastic and diffusion fields. This view characterizes the morphological stability calculations of Leo and Sekerka [10]. If the kinetic processes governing the transformation are allowed to reach an end state, the kinetically driven shapes should match the equilibrium shapes [11].

In this paper, we adopt the kinetic based approach to study the problem of the morphological evolution of an initially cylindrical precipitate growing by diffusion in a binary crystalline alloy, when arbitrary loads are applied during the transformation. We also allow for an arbitrary misfit between the precipitate and the surrounding matrix. The precipitate and matrix are

1

taken to be elastically isotropic, but with different elastic moduli.

We pose the problem as an initial value problem for the diffusional growth of an infinitely long cylindrical precipitate. At some time $t = 0$ after the nucleation of the precipitate and before any Mullins–Sekerka morphological instabilities occur [12], we subject the system to an applied stress. As noted by Johnson [13], these stresses will immediately interact with the diffusion fields, so that the cross-section of the precipitate will not in general remain circular. The goal of the analysis presented here is to describe the evolution of the precipitate by developing a coupled set of partial differential equations and boundary conditions for the stress and diffusion fields throughout the material, which in turn yield the speed of the moving interface.

In order to keep the problem tractable, we assume that the system is always near equilibrium, so that the equations of elastostatics can be used to find the stress fields in the system. Also, we use the equilibrium equations derived from the thermodynamics of solids to develop a diffusion equation and a boundary condition for the composition of the diffusing species. We neglect surface stress and we take the atomic volumes of the two components to be identical. The latter assumption allows us to neglect both stress-assisted diffusion and coupling between the elastic and diffusion fields [14]. Finally, following Mullins and Sekerka's analysis of the morphological stability of a sphere [12] and Coriell and Parker's similar analysis of a cylinder [15], we consider a small but otherwise arbitrary perturbation off of the initially unperturbed cylinder, and we only retain terms that are first order in the perturbation amplitude.

The outline of our analysis is as follows. We first calculate the detailed stress and strain fields that arise from a combination of applied load and misfit. The elastic fields are used to find the diffusion fields everywhere in the system, which in turn yield the local normal growth speed of the interface.

2

Finally, we use this interfacial speed to determine the evolution of the growing precipitate.

2 Elastic Fields

2.1 Unperturbed Cylinder

Consider a cylindrical inclusion of radius R embedded in a matrix of infinite extent. We take a coordinate system such that the cross-section of the cylinder lies in the $x_1 - x_2$ plane, and the x_3~direction coincides with the axis of the cylinder. The inclusion phase has shear modulus μ^I and Poisson ratio $i/$, while the corresponding constants of the matrix phase are μ^M and v^M. Suppose that there is a constant misfit e_{ij}^* between the two phases, and that there is a uniform far-field stress σ_{ij}^∞ (or a far-field strain e^∞) in the matrix. Finally, suppose $i,j = 1,2$ only, so that both the far-field stresses and the misfit only act in the plane normal to the axis of the cylindrical inclusion, and assume there is no displacement in the x_3-direction. Then, we have a combination of Eshelby's transformation and inhomogeneity problems in the framework of plane strain elasticity [16].

In order to account for the misfit, we take as our reference state an imaginary state after the transformation has occurred, in which the inclusion has been stressed so as to retain its original shape and size, and the matrix is stress free. The constitutive equations relating stress σ_{ij} and strain e_{ij} are given by $\sigma_{ij} = C_{ijkl}^I(e_{kl}^I - e_{kl}^*)$ in the inclusion, and $\sigma_{ij}^M = C_{ijkl}^M e_{kl}^M$ in the matrix, where e_{ij} is the infinitesimal strain tensor and C_{ijkl} denotes the isotropic stiffness tensor. These stresses must satisfy the equations of elastic equilibrium in the absence of body forces, $d\sigma_{ij}/dx_j = 0$.

The boundary conditions that apply at the inclusion-matrix interface

3

correspond to those at a coherent crystal-crystal interface [17]. Therefore, at the interface $r = \sqrt{x^2 + y^2} = R$ the displacements are continuous, $u_i^I = u_i^M$, and the tractions are continuous, $\sigma_{ij}^I n_j = \sigma_{ij}^M n_j$, where the unit normal $n = \{n_j\}$ is taken to point from the inclusion to the matrix. Finally, we must satisfy the appropriate far-field conditions on stress or strain as $r \to \infty$, and we insist that the displacement is bounded as $r \to 0$.

To find a solution to the above problem, we express the far-field stresses or strains and the misfit strain in polar coordinates (r, θ). If we imagine splitting the far-field strain into its hydrostatic and deviatoric components, then the hydrostatic component (say $\bar{\epsilon}$) corresponds to a purely radial displacement $u_r = \bar{\epsilon} r$, $u_\theta = 0$ in polar components, while the deviator corresponds to a displacement of the form $u_r = ar \, \cos(2\theta - \phi)$, $u_\theta = -ar \, \sin(2\theta - \phi)$, where a is the magnitude of the deviatoric strain and ϕ is some constant phase angle. These far-field displacements serve as a template to find the particular form of the solution to the equations of elastic equilibrium that satisfy the boundary conditions.

As a simple example, consider the problem where there is no misfit and the applied strain is a pure shear $\epsilon_{11}^{app} = -\epsilon_{22}^{app}$, $\epsilon_{12}^{app} = 0$. (This problem, as well as problems with hydrostatic loading or misfit, has been considered in reference [18], among others.) This shearing strain corresponds to far-field displacements $u_r = ar \, \cos 2\theta$ and $u_\theta = -ar \, \sin 2\theta$. In order to match this far-field condition, we use either the series solution given by Alexander et al. [19] or the Airy's stress potentials [20] to find an equilibrium displacement field with components in polar coordinates that are proportional to $\cos 2\theta$ and $\sin 2\theta$. After satisfying the boundary conditions, we find

$$u_r^{I(0)} = \frac{\omega(4 - 4\nu^M)}{3 + \omega - 4\nu^M} \left(\frac{r}{R}\right) Ra \cos 2\theta, \tag{1}$$

$$u_\theta^{I(0)} = -\frac{\omega(4 - 4\nu^M)}{3 + \omega - 4\nu^M} \left(\frac{r}{R}\right) Ra \sin 2\theta, \tag{2}$$

4

$$u_r^{M(0)} = \left[\left(\frac{r}{R}\right) + \alpha_2 \left(\frac{R}{r}\right)^3 - \alpha_2(4 - 4\nu^M)\left(\frac{R}{r}\right)\right] Ra\cos 2\theta \qquad (3)$$

and

$$u_\theta^{M(0)} = -\left[\left(\frac{r}{R}\right) - \alpha_2 \left(\frac{R}{r}\right)^3 - 2\alpha_2(1 - 2\nu^M)\left(\frac{R}{r}\right)\right] Ra\sin 2\theta, \qquad (4)$$

where $\omega = \mu^M/\mu^I$ is the ratio of the shear moduli of the matrix and inclusion, $\alpha_2 = (1 - \omega)/(3 + \omega - 4\nu^M)$ and the '0' superscript refers to the unperturbed problem.

2.2 Perturbed Cylinder

Consider the same elasticity problem as above, but suppose that the interface between the precipitate and the matrix has the shape of a perturbed cylinder,

$$r(\theta) = R + \delta \cos n\theta, \qquad (5)$$

where $|\delta/R| \ll 1$ so that terms of order $|\delta/R|^2$ and higher can be neglected. For simplicity, we consider here a single n–fold perturbation mode, though later we will need to consider all perturbation modes.

We write the total displacement in the inclusion–matrix system as

$$\mathbf{u}(r,\theta) = \mathbf{u}^{(0)}(r,\theta) + \left(\frac{\delta}{R}\right)\mathbf{u}^{(1)}(r,\theta) \qquad (6)$$

where the displacement $\mathbf{u}^{(0)}$ associated with the unperturbed cylinder is known from the results of Section 2.1, and we have to find the displacement $\mathbf{u}^{(1)}$ arising from the shape perturbation. We take this perturbed displacement to be of the form [19]

$$u_r^{(1)}(r,\theta) = \left[A_1 r^2 + B_1 + Cr^{-2} + D_1 \ln r\right]\cos\theta \qquad (7)$$

$$+ \sum_{k=2}^{\infty}\left[A_k r^{k+1} + B_k r^{k-1} + C_k r^{-(k+1)} + D_k r^{-(k-1)}\right]\cos k\theta$$

and

$$u_\theta^{(1)}(r,\theta) = \left[\alpha_1 A_1 r^2 - B_1 + C_1 r^{-2} - D_1 \ln r - \frac{1}{3 - 4\nu^\bullet} D_1\right] \sin\theta \qquad (8)$$

$$+ \sum_{k=2}^{\infty} \left[\alpha_k A_k r^{k+1} - B_k r^{k-1} + C_k r^{-(k+1)} + \beta_k D_k r^{-(k-1)}\right] \sin k\theta.$$

where

$$\alpha_k = \frac{4(1 - \nu^\bullet) + k}{2(1 - 2\nu^\bullet) - k}, \quad \beta_k = \frac{k - 4(1 - \nu^\bullet)}{2(1 - 2\nu^\bullet) + k} \qquad (9)$$

for all $k \geq 1$, where '$\bullet$' can be either 'I' or 'M'.

Even though we are considering a single $\cos n\theta$ shape perturbation, the perturbed displacements will include other cosine modes because of the applied fields. Hence we keep the summation on k in eqns. (7) and (8). The particular values of k that the system selects, as well as the constants A_k through D_k, are determined by insuring that the total displacement (6) satisfies the far–field conditions and the boundary conditions evaluated at the interface (5). The resulting expressions are linearized in δ/R to derive conditions for the order δ/R part of the total displacement. Since the unperturbed displacement already satisfies the far–field condition, the perturbed displacement must vanish as $r \to \infty$, and must remain finite at $r = 0$. The linearization of the boundary conditions at the precipitate–matrix interface can be illustrated by evaluating the equation expressing the continuity of u_r at $r(\theta) = R + \delta \cos n\theta$, and expanding in powers of δ/R. We find that the zeroth order contribution is $u_r^{M(0)}(R) = u_r^{I(0)}(R)$, which is satisfied by the solution to the unperturbed problem, while the first order contribution yields

$$u_r^{M(1)}(R) - u_r^{P(1)}(R) = \left(\frac{\partial u_r^{P(0)}(R)}{\partial r} - \frac{\partial u_r^{M(0)}(R)}{\partial r}\right) \cos n\theta. \qquad (10)$$

Since $u_r^{P(0)}$ and $u_r^{P(0)}$ are known from the solution to the unperturbed problem, this equation specifies the jump in the r–component of the perturbed

6

displacement. Similar expansions for the θ-component of the displacement and the two components of the balance of tractions prescribe the remaining boundary conditions for the perturbed problem.

The linearized boundary condition (10) also reveals how we determine the values of k needed for the perturbed displacements (7) and (8). Recall that the unperturbed displacement u_r^0 may be written as a function of radius only, which corresponds to hydrostatic loading, plus a function proportional to $\cos 2\theta$, which corresponds to pure shear. Thus, the right hand side of eqn. (10) includes a $\cos n\theta$ term plus a term proportional to $\cos 2\theta \cos n\theta = \frac{1}{2}[\cos(n+2)\theta + \cos(n-2)\theta]$. It is easy to see that the same reasoning applies to the remaining boundary conditions, so that we must choose $k = n$, $n - 2$, $n+2$ for the perturbed displacements (7) and (8). Finally, the constants A_k through D_k for these k's are found by satisfying the complete set of linearized boundary conditions. We note that some care must be taken when $n = 2$ and $n = 3$, since these correspond to special cases of the general solution (7) and (8).

3   Diffusion Fields

Consider a perturbed cylinder growing from a supersaturated matrix. The concentration in the precipitate is taken to have a uniform value C, the far-field concentration is given by c_∞, and the concentration at the precipitate-matrix interface is denoted by c_s. We assume that the concentration fields reach steady state at every stage in the precipitate growth, so that the diffusion equation reduces to Laplace's equation. This quasi-static approximation is valid if the growth speed of the precipitate is slower than the characteristic speed of diffusion, which is the case if the supersaturation $S = |(c_\infty - c_s)/(C - c_s)| \ll 1$.

Because the solution to Laplace's equation in two-dimensions has a logarithmic component, adopting the quasi-static approximation requires one to introduce a finite outer boundary for the diffusion field [15]. This finite outer boundary, R_x, may be found from $R_1 = R/(v_1)$, where $\ln i_1^2 = 0.5772$ is Euler's constant and A is found by solving $A^2\ln(i_1^2 A^2) + 5 = 0$. Since the supersaturation S is small, A will be small and so $R_1 \gg R$. We note in this regard that in the calculation of the elastic fields in Section 2, we took the outer boundary to be at infinity. However, as long as $R_1 \gg R$ this introduces negligible errors.

The concentration c_s at the precipitate-matrix interface is found by extending the equilibrium conditions at a coherent crystal-crystal interface to the precipitate growth problem [17]. The detailed calculation of this boundary condition has been described previously [10]; the result is

$$c_s = co \left[1 + *(*7 + G*)\right],\qquad\qquad (11)$$

where Co is the matrix concentration at an incoherent planar interface and $z = (1 - X)/(k_9 Tp\backslash X - xoj)$, where xo and X are the mole fractions corresponding to Co and C, p is the density of the alloy, k_g is the gas constant and T is absolute temperature. Also, 7 is the interfacial energy, which is assumed to be constant, K is the local mean curvature of the interface, taken so that $K = \backslash/R$ for a circle of radius R, and

$$G^{el} = \frac{1}{2} b_{ijki} a_{ij} a_{ki} - \frac{1}{2} \varepsilon_{«w} \cup_{«} \cup_{kl} - \left(\epsilon_{ij}^M - \epsilon_{ij}^I\right)\sigma_{ij}^M \qquad\qquad (12)$$

is the elastic contribution to c_5, where S_{ijki} indicates the components of the elastic compliance tensor. Roughly, $C^{e/}$ is a pointwise measure of the elastic energy densities of the two phases and the work needed to keep the interface coherent through any transformation.

The interfacial concentration c_s depends on the angle 6 through both the curvature K and the elastic energy density G^{el}. For the shape (5), we find

that to order δ/R, $\kappa = 1/R + \delta(n^2 - 1)\cos n\theta/R^2$, so that κ depends on θ only through the shape perturbation. The elastic energy density G^{el} depends on θ not only through the shape perturbation, but also through the angular dependence of the applied stress. From the calculation of the elastic fields, we can show that the general form of G^{el} is

$$G^{el} = G_0 + G_2 \cos 2\theta + G_4 \cos 4\theta \qquad (13)$$
$$+ \frac{\delta}{R} \{ G_{n-4}\cos(n - 4)\theta + G_{n-2}\cos(n - 2)\theta$$
$$+ G_n \cos n\theta + G_{n+2}\cos(n + 2)\theta + G_{n+4}\cos(n + 4)\theta \} .$$

Obviously, the details of the applied stress, misfit and elastic constants lead to different coefficients G_2, G_4, G_n, $G_{n\pm2}$ and $G_{n\pm4}$. There are, however, two important features inherent in the form of eqn. (13). The first is that G^{el} depends on θ even when $\delta = 0$. Johnson [13] found an equivalent result in the case of a spherical precipitate under uniaxial tension, and concluded that an initially spherical precipitate would not grow as a sphere. A second, related observation is that while the order δ/R contribution to G^{el} has one contribution, $G_n \cos n\theta$, that is 'in-phase' with the shape perturbation, all the remaining contributions are 'out-of-phase' with the shape perturbation. The out-of-phase contributions arise from the interaction between the shear component of the applied stress (or misfit) and the shape of the precipitate, and are not present when hydrostatic pressures or dilatational misfits are the only sources of stress in the system.

Finally, the concentration field is given by the solution to Laplace's equation,

$$c(r) = A + B \ln r \qquad (14)$$
$$+ (C_2 r^{-2} + D_2 r^2)\cos 2\theta + (C_4 r^{-4} + D_4 r^4)\cos 4\theta$$
$$+ \frac{\delta}{R}\left[\sum_k \left(E_k r^{-k} + F_k r^k \right)\cos k\theta + G \ln r \right],$$

where $k = n$, $n \pm 2$ and $n \pm 4$ and the constants A, B, C_2, D_2, C_4, D_4, E_k,

F_k and G are found from the far-field condition that $c \to c_\infty$ at $r = R_\lambda$ and the boundary condition (11), evaluated at the interface (5) and linearized in δ/R. We will not present the details of this calculation here.

4 Shape Evolution

The motion of the precipitate–matrix interface is determined by its normal growth speed v_n, which is given by the flux balance

$$v_n = \frac{d}{dt} r(\theta, t) = \frac{D}{C - c_s(\theta)} \nabla c \cdot \hat{n} \,|_{\text{interface}}, \tag{15}$$

where $r(\theta, t)$ is the position of the interface at any time t. Suppose we view the evolution of the precipitate as an initial value problem where the shape at some time t_0 is given by $r = R_0 + \delta \cos n\theta$, as in eqn. (5). From the discussion following eqn. (13), it is clear that it will not be sufficient to take a growth speed of the form $v_n = dR_0/dt + (d\delta/dt) \cos n\theta$. Thus, in evaluating eqn. (15), we take

$$r(\theta, t) = R(t) + \sum_k b_k(t) \cos k\theta, \tag{16}$$

where $R(t = t_0) = R_0$ and $b_k(t = t_0) = \delta$ if $k = n$ and vanishes otherwise. We insist that $|b_k(t)/R(t)| \ll 1$ so that the results of the previous sections apply to the evolving shape. To calculate the normal growth speed at $t = t_0$, we evaluate the right hand side of the flux balance (15) by using the concentration field found in Section 3, and set the result equal to the time derivative of eqn. (16). For a general applied stress and misfit, the unperturbed cylinder generates *three* growth terms, $\dot{R}$, $\dot{b}_2$ and $\dot{b}_4$, while the perturbation $\delta \cos n\theta$ induces up to *five* growth modes, $\dot{b}_{n\pm4}$, $\dot{b}_{n\pm2}$ and $\dot{b}_n$.

We call $\dot{R}$ and $\dot{b}_n$ the fundamental growth modes because they arise directly from the shape (5). By following the procedure described above, we find that $\dot{R}$ and $\dot{b}_n$ are similar in form to the values of $\dot{R}$ and $\dot{\delta}$ reported by

Leo and Sekerka [10]. In particular, $\dot{b}_n$ includes a positive contribution from the supersaturation, which is associated with the point effect of diffusion, a negative contribution from capillarity, and a contribution from elasticity that is proportional to G_n and can be either positive or negative.

However, unlike the Leo-Sekerka problem, the evolution of the precipitate shape also includes the modes $\dot{b}_2$, $\dot{b}_4$, $\dot{b}_{n\pm4}$ and $\dot{b}_{n\pm2}$. These stress-induced modes are generated by both the unperturbed cylinder and the shape perturbation. The growth modes $\dot{b}_2$ and $\dot{b}_4$ arise in the unperturbed problem owing to the elastic energy densities G_2 and G_4 (see eqn. (13)). Similarly, $\dot{b}_{n\pm4}$ and $\dot{b}_{n\pm2}$ result from the initial n–fold perturbation through the elastic energy densities $G_{n\pm2}$ and $G_{n\pm4}$.

In light of the above discussion, we may imagine the following scenario for the evolution of a precipitate. Suppose that at some time after the nucleation of a cylindrical precipitate, we apply a uniform far-field stress to the system. We see from the above analysis that the cylinder will immediately be unstable, and will develop in general both two– and four–fold perturbations off of its circular cross-section. As the growth process continues and these initial perturbations grow, they induce six– and eight–fold perturbations, which in turn induce 10- and 12-fold perturbations, and so on. Stabilization of the induced modes occurs when their amplitude becomes large enough so that capillary effects begin to slow their growth.

Therefore it is clear that a cylindrical precipitate will be an unstable growth shape when the system is under applied stress. The obvious question is, can we find a shape that is stable for some range of sizes? Consider again the fully perturbed shape given by (16), only now at some time when all the perturbation modes have some amplitude. Since each perturbation amplitude b_k will generate up to five growth modes or, equivalently, each growth mode depends on up to five perturbation amplitudes, we have a linear system of

11

equations,

$$\dot{R} = a_{00}H + 002^\wedge 2 + O0464$$

$$\dot{6}1 = 01161 + 01363 + 01565$$

$$\dot{6}2 = CL20R + O2262 \sim {}^a24\&4 + a_{26}b_6$$

$$\dot{6}3 = CI3161 + 03363 + 03565 + 03767 \qquad (17)$$

$$\dot{6}4 = a^\wedge R + 04262 + 04464 + O4666 + a_{48}b_8$$

$$\vdots$$

$$\dot{b}_k = a_{k,k-4}b_{k-4} + a_{k,k-2}b_{k-2} + a_{k,k}b_k + a_{k,k+2}b_{k+2} + a_{k,k+4}b_{k+4}$$

$$\vdots$$

where the diagonal terms *akk* (no sum) are associated with the fundamental growth modes and the off-diagonal terms O_i ($z^\wedge j$) with the stress-induced modes. The coefficients $a_{»j}$ depend on the radius -R; however, consistent with the the quasi-static assumption, we take R to be fixed at any instant in time.

The system of equations (17) is an infinite dimensional matrix equation $\dot{x} = Ax$, where the vector x = {#,61,62,...} and the matrix A = [ay]. The question of the morphological stability of the precipitate is answered by studying the eigenvalues and eigenvectors of the matrix A.

As an aside, we note that in the context of the Mullins-Sekerka analysis [12], the matrix A is a diagonal matrix. The first term of the matrix, ooo, is the positive eigenvalue corresponding to the supersaturation driven growth of the cylinder (i.e., the eigenvalue {/?,0,0,...}). The next eigenvalue, $022,^1$ is exactly the ratio $\dot{6}2/62$ that determines the stability of the two-fold growth mode (eigenvector {0,62,0,0,...}). The same ideas apply to the nth eigenvalue o_{nn} and eigenvector {0,0,...,6_n,0,.•.}.

Returning to the the problem at hand, we see that because stress-induced

_____

[1]**A one-fold perturbation corresponds to a translation of the circle, and so is not considered.**

12

coupling leads to off-diagonal terms in A, its eigenvalues and eigenvectors cannot be directly determined by inspection. However, we expect to find the following behavior. At small enough precipitate sizes, there will be a single positive eigenvalue associated with the supersaturation. The corresponding eigenvector will not be simply $\{\#, 0, 0, \dots\}$, but will be of the form $\{H, 0, 62)0, 6_4, \dots\}$ to reflect the fact that the cylinder generates two- and four-fold growth modes and so on. (The form of the G^{el} term in eqn. (13) implies that the applied stresses couple even perturbation modes to other even modes, or odd modes to other odd modes.) The stability of this 'base' state is determined by the remaining eigenvalues and eigenvectors, which are functions of the size of the precipitate.

Thus, there are now two separate problems to consider. First, we need to understand the base shapes associated with the first eigenvalue of the matrix A. We then calculate when these shapes are stable.

4.1   The Base Shape

Let the first eigenvalue of the matrix A be denoted f_0 where it is straightforward to show that $£0$ is a positive number directly related to the supersaturation. Let the eigenvector associated with f_0 be given by $\{i?, 0, b_2^{(\partial)}, 0, 6_4^{(0)}, \dots\}$, where the particular values of $bf\setminus \&4$- $\cdot \cdot$ depend on R, the applied stress, the misfit and the elastic constants of the precipitate and matrix phases.

At any instant in time, we define a base shape

$$r^{(o)}(0,i) = R(t) + f > £?(t)\cos 2/c0, \qquad (18)$$

consisting of small perturbations off a circle. We will show in Section 4.2 that this base shape is instantaneously stable in the sense that if we take a fixed value of R less than some critical value, all small perturbations off (18) decay. However, as growth continues and R increases, the base shape

13

amplitudes $b_{2k}^{(0)}$ change. In other words, eqn. (18) defines a set of shapes that evolve in time through the radius $R(t)$.

Consider the following interpretation of the base shape (18). If we let $\mathbf{x}^{(0)}$ be the eigenvector associated with ξ_0, so $\mathbf{x}^{(0)} = \{R, 0, b_2^{(0)}, 0, b_4^{(0)}, \ldots\}$, then the evolution of the base shape is governed by the matrix equation $\dot{\mathbf{x}}^{(0)} = \mathbf{A}\mathbf{x}^{(0)} = \xi_0\mathbf{x}^{(0)}$. If we restrict attention to values of R less than the above mentioned critical radius, then ξ_0 will be the largest positive eigenvalue of $\mathbf{A}$, and so $\mathbf{x}^{(0)}$ is the fastest growing eigenvector. Equivalently, the base shape (18) is the fastest growing shape among all possible shapes of the form (16). However, because $\mathbf{A}$ depends on R, the progression of base shapes as R increases will not in general be self-similar.

In order to calculate the eigenvalues and eigenvectors of the infinite-dimensional matrix $\mathbf{A}$, we truncate the system of equations (17) at some large value of k and calculate the eigenvalues and eigenvectors of the resulting finite matrix. We then change the upper limit of k and recalculate the eigenvalues in order to insure that any truncation errors are small. It turns out that the perturbation amplitudes $b_{2k}^{(0)}$ of the base shape decrease rapidly with k, so truncation errors are negligible.

We now discuss some detailed calculations of the base shapes for different applied loads and combinations of elastic constants. We consider only applied shears and applied uniaxial tensions, and we limit ourselves to dilatational misfit strains. While more general cases can be considered, most of the interesting physics can be seen in these relatively simple cases. In all the figures, we choose dimensionless groups such that the elastic constants of the matrix are fixed and those of the precipitate vary. Also, the radius R is normalized by $R^* = z\gamma c_0/(c_\infty - c_0)$, which is the critical nucleus radius for a cylindrical precipitate.

Because our main purpose is to highlight the role of applied stress and

elastic constants on the growth of a precipitate, we set the supersaturation at about 0.8% by choosing $\ln(R_\lambda/R) = 3$. Higher supersaturations lower the critical nucleus radius R^* and hence increase the importance of capillarity. Therefore, for a given value of R/R^*, elastic effects will be weaker at higher supersaturations, and so the base shapes will be closer to a circle. We note that for the parameters we have chosen, the base shapes in some cases have a maximum perturbation amplitude of up to about 20% of the radius R.

Consider first the case of applied stress and zero misfit. The first observation is that if the shear moduli of the precipitate and matrix are equal ($\omega = \mu^M/\mu^I = 1$), the base shape is a circle. This result agrees with the calculations of Berkenpass et al. [5], which show that the elastic energy of an elliptic cylinder under applied tension is independent of aspect ratio when the shear moduli of the cylinder and the surrounding matrix are equal. We also observe that at fixed $\omega \neq 1$, the base shapes depend very weakly on the Poisson ratios of the precipitate and matrix. Thus all our figures for the base shapes are plotted for the case where the two phases have the same Poisson ratio. However, we note that the Poisson ratios will be important in studying the stability of the growing precipitate, even when $\omega = 1$.

If the shear moduli of the precipitate and matrix differ, then the base shape will differ from a cylinder. Figures 1 and 2 each show a progression of base shapes for three values of R/R^*, when the system is under an applied shear $\sigma_{11}^{app} = -\sigma_{22}^{app}$, $\sigma_{12}^{app} = 0$ with zero misfit. In Fig. 1, $\omega = 0.5$, so the precipitate phase has a higher shear modulus than the matrix, while in Figure 2, $\omega = 2$, so the opposite is true. The base shapes in both figures differ substantially from a circle, and exhibit a four-fold symmetry that reflects the symmetry of the strain energy density in pure shear. By comparing Figs. 1 and 2, we find that the deviations from a circular shape are more pronounced when the precipitate has a lower shear modulus that the matrix. This observation agrees in principle with the conclusion of Leo and Sekerka

15

that the elastic fields arising from a dilatational misfit tend to destabilize a 'soft' (low shear modulus) precipitate, and tend to stabilize an elastically 'hard' precipitate [10].

Figures 1 and 2 also show that as R/R^* increases and the stabilizing effect of capillarity lessens, the base shape moves progressively away from a circle. Since in the quasi-static limit time changes via $R(t)$, we view the progression of shapes in Figs. 1 and 2 as possible kinetic paths for the transforming system. As long as the base shape is stable, these kinetic paths are paths of fastest growing shapes. We note that all the shapes shown in Figs. 1 and 2 are well within the linear stability regime (see Section 4.2), though nonlinearities may become significant well before the onset of linear instability.

The same basic conclusions hold when we consider a uniaxial tension. Figures 3 and 4 show a progression of base shapes under an applied uniaxial tension σ_{11}^{app} and zero misfit for $\omega = 0.5$ and 2, respectively. As in the applied shear case, the deviation of the base shape from a circle is more pronounced when the precipitate has a lower shear modulus than the matrix. However, we now find that because uniaxial tension has a hydrostatic component, the strain energy density has two-fold symmetry. Hence the base shapes under tension are approximately elliptical, as opposed to the more squarish shapes seen in the applied shear case. Further, the long axis of the precipitate is perpendicular to the axis of applied stress, in agreement with the energy calculations of Berkenpass et al. [5].

The results above can be altered drastically by combining applied stress with dilatational misfit strains. Figure 5 shows the base state evolution for applied shear and positive misfit. Because the misfit adds a hydrostatic component to the elastic fields, the base shapes take on more of the elliptic shape seen in the uniaxial tension case. The positive misfit tends to align the growing precipitate in the vertical direction (recall that the applied shear

corresponds to tension in the horizontal direction and compression in the vertical direction). In contrast, if we were to take a negative misfit, the precipitate would align horizontally, in a 90° rotation of the shapes shown in Fig. 5.

Consider finally the interaction between dilatational misfit and applied tension. A positive misfit combined with uniaxial tension simply accentuates the patterns seen in uniaxial tension alone. However, the orientation of the precipitate growing under tension may be changed by imposing a large enough negative misfit strain. Figure 6 shows the effect of increasing the magnitude of the negative misfit. As the magnitude if the misfit increases, the base shape moves from a shape whose long axis is perpendicular to the applied tension (Fig. 4), through a shape that is approximately circular (Fig. 6a), and into a shape with a long axis parallel to the applied stress (Fig. 6b). If we consider compression instead of tension, then we need a positive misfit to alter the orientation of the evolving base shape. Again, these results are in basic agreement with energy calculations, although the energy calculations indicate a sharp transition in the orientation of the precipitate as the misfit changes sign, rather than the smooth transition observed here.

4.2 Stability of the Base Shape

As has just been discussed, the first eigenvalue fo of the matrix A is always positive, and is associated with the evolving base shape. The remaining eigenvalues & and eigenvectors $x^{(*\}}$ $k \geq 1$, are associated with perturbations off this base shape, and so determine the stability of the base shape. Following Mullins-Sekerka [12], we can consider two viewpoints of the stability of the growing precipitate. In the first, we focus on whether the perturbations grow or decay, and so we consider the signs of the eigenvalues £* as a function of the radius R. Alternately, we can ask whether the perturbations change the

shape of the evolving precipitate, which requires looking at sign of $\xi_k - \xi_0$ for each $k \geq 1$, again as a function of R. Both stability criteria lead to a critical value of R for each $k \geq 1$. In what follows, we adopt the shape stability criterion and calculate the critical radius at which ξ_k overtakes ξ_0.

Because we are considering the linear stability of a time–dependent base shape that is itself a small amplitude perturbation off a circle, we must choose parameters that ensure that the perturbation amplitudes of the base shape at the critical radius for instability are small. Here, in order to fully explore the roles of elastic constants and applied stress on the stability of the evolving base shape, we allow for perturbation amplitudes in the base shape of up to about 10% before we concede that nonlinearities have taken over the dynamics of growth.

As in the calculation of the base shapes, we fix the supersaturation by setting $\ln(R_\lambda/R) = 3$. As discussed by Coriell and Parker [15], this value affects the critical radius for instability such that the critical radius decreases as $\ln(R_\lambda/R)$ decreases (supersaturation increases). Also, as mentioned earlier, elastic effects become less important as the supersaturation increases. However, the results we present here are qualitatively valid for all supersaturations we have considered.

In all the cases we have studied, we find that ξ_3 is the first eigenvalue to become larger than ξ_0. As R increases above the critical radius for which the perturbation shape $\mathbf{x}^{(3)}$ goes unstable, we find a strictly monotone progression of unstable modes—i.e., $\mathbf{x}^{(4)}$ goes unstable, followed by $\mathbf{x}^{(5)}$, and so on. We never see an instability associated with $\mathbf{x}^{(1)}$, which is essentially a translation of the circle. We also never see an instability associated with $\mathbf{x}^{(2)}$, even though the base shape includes a two–fold perturbation.

The critical radius $R_{cr}(3)$ at which ξ_3 becomes greater than ξ_0 depends on the elastic constants, applied field and misfit. Figure 7 shows a plot of

$R_{cr}(3)/R^*$ as a function of ω when the Poisson ratios of the two phases are the same, and the system is subjected to an applied shear and three different misfits. The critical radius is a strong function of ω, such that stability is favored for $\omega < 1$ (a 'hard' precipitate) and instability is favored for $\omega > 1$ (a 'soft' precipitate). Adding misfit leads to a small destabilization of the system that is independent of the sign of the misfit. In the zero misfit case, the value of $R_{cr}(3)/R^*$ when $\omega = 1$ is exactly equal to that calculated by Coriell and Parker in the absence of stress [15]. However, when a misfit is present, the value of $R_{cr}(3)/R^*$ at $\omega = 1$ is no longer at this zero stress value, though the deviation is very small.

If we put the system under applied tension, we again come to the conclusion that the stability of the base shape decreases as ω increases. Figure 8 shows $R_{cr}(3)/R^*$ versus ω for three values of misfit. In contrast to the applied shear case, the sign of the misfit is important, with a positive misfit being stabilizing and a negative misfit being destabilizing. As in the applied shear case, when $\omega = 1$ we recover the Coriell–Parker critical radius only for vanishing misfit.

Figures 7 and 8 are both for the case where the Poisson ratios of the precipitate and matrix are equal. Of fundamental interest is what happens when the Poisson ratios of the two phases are different, so the system is elastically inhomogeneous even though ω may be unity. Figure 9 shows $R_{cr}(3)/R^*$ versus ω for different combinations of Poisson's ratios, when the system is under tension and has zero misfit. As ν^I decreases below ν^M, there is a destabilization of the base shape, even when $\omega = 1$. In contrast, there is a stabilization of the system as ν^I increases above ν^M.

A nice interpretation of the above results can be found by casting them in terms of bulk moduli rather than Poisson ratio. Figure 10 shows $R_{cr}(3)/R^*$ as a function of the bulk modulus ratio K^M/K^I for different values of ω, again

for the uniaxial tension and zero misfit case. The $\omega = 1$ curve shows clearly that there elastic fields affect stability when the bulk moduli of the two phases differ. Further, we observe the rough trend that the bulk modulus stabilizes the system when $K^M < K^I$ and destabilizes the system when $K^M > K^I$. There is some sense of more complicated behavior as ω moves away from one; however, by this point we may be neglecting significant nonlinear effects.

Our conclusion is therefore that the ratios of both the bulk and shear moduli affect the stability of the base shape, with the trend being that if the precipitate has the higher modulus there is a stabilizing effect, while if the precipitate has a lower modulus there is a destabilizing effect. The relative importance of the moduli ratios depends on the details of the applied fields and misfit. For example, in the cases of applied shear only or dilatational misfit only, only the shear modulus ratio ω enters the stability results. In other cases, both the shear and bulk moduli ratios are needed to fix the stability picture.

5   Further Discussion and Summary

The introduction of applied stresses in an analysis of the morphological evolution of a growing precipitate leads to problems that are not apparent when only simple dilatational misfits are considered. As has been recognized previously [13], the applied fields in general break the symmetry of the problem, so that a growing circular cylinder is not a solution to the field equations. In the context of a linear morphological stability analysis, this implies that we have to look for a base shape with a cross-section that deviates slightly from a circle, and then consider further small perturbations off that shape in order to test for stability.

The base shapes depend on the details of the applied field and misfit,

as well as on the ratio of the shear moduli of the matrix and precipitate. This dependence is determined by the angular variation of the strain energy density at the precipitate–matrix interface. Thus, we find that with no misfit, the base shapes under an applied shear differ from those with under a uniaxial tension. By adding misfit to the system, we can change both the symmetry of the base shape, as well as its orientation relative to the applied stress. For all cases, the base shape degenerates to a circle if the ratio $\omega = \mu^M / \mu^I = 1$. If $\omega \neq 1$, then the deviation of the base shape from a circle is larger if $\mu^I < \mu^M$, while the base shape stays closer to a circle if $\mu^I > \mu^M$.

We find a strong qualitative similarity between our evolving base shapes and the precipitate shapes calculated in [5]. Our base shapes also compare qualitatively with equilibrium shapes calculated for elastically homogeneous but anisotropic systems [8, 9]. We expect that the introduction of anisotropy breaks the symmetry associated with a circular base shape, much as applied stress does in an elastically isotropic system. In other words, the elastic fields that arise in an anisotropic system will couple different mode shapes in much the same way that applied stresses do in our analysis.

As has been discussed, a stable base shape is a fastest growing shape. We have run some simple numerical simulations involving updating the interface via the normal growth speed (15). These calculations show that at least in the linear perturbation regime, an initially circular precipitate will very quickly reach the appropriate base shape and subsequently evolve along a path of base shapes. The paths we have calculated should be valid until nonlinearities begin to appear, so $|\delta/R|^2$ terms become significant, or until the base shape itself becomes unstable.

The onset of instability of the base shape itself depends strongly on the elastic constants of both phases and the details of the elastic fields. The base shape is stabilized when the shear modulus of the precipitate is higher than

21

that of the inclusion, and destabilized when the opposite is true. However, the stability picture when applied stresses are present also depends on the bulk moduli of the two phases. We find that even when the shear moduli of the precipitate and matrix are the same, there is an elastic influence on the critical radius for instability when the bulk moduli of the two phases differ. As with the shear moduli, we conclude that all else being equal, the base shape is stabilized if the bulk modulus of the precipitate is higher than that of the inclusion, and destabilized in the alternate case.

Acknowledgements

References

[1] V. Bliss and D.L Sponseller, *Met. Trans.* 4, 1953 (1973).

[2] J. Conley, M.E. Fine and J.R. Weertman, *Acta rnetall* 37, 1251 (1989).

[3] J.K. Tien and S.M. Copley, *Met. Trans.* 2, 215 (1971).

[4] T. Miyazaki, K. Hakamura and H. Mori, *J. Mater. Sci.* 14, 1827 (1979).

[5] M.B. Berkenpas, W.C. Johnson, and D. E. Laughlin, *J. Mater. Res.* 1, 635 (1986).

[6] W. C Johnson, M. B. Berkenpas and D. E. Laughlin, *Acta rnetall* 36, 3149 (1988).

[7] M.A. Grinfeld, *Priki Matem. Mekhan. USSR* 51, 489 (1987).

[8] I.M. Kaganova and A.L. Roitburd, *Sov. Phys. JETP* **67**, 1173 (1988).

[9] M. McCormack, A.G. Khatchaturyan and J.W. Morris, *Acta metall.* **40**, 325 (1992).

[10] P.H. Leo and R.F. Sekerka, *Acta metall.* **37**, 3139 (1989).

[11] P.W. Voorhees, G.B. McFadden and W.C. Johnson, to appear in *Acta metall.*.

[12] W. W. Mullins and R. F. Sekerka, *J. Appl. Phys.* **34**, 323 (1963).

[13] W. C. Johnson, *Met. Trans.* **18A**. 233 (1987).

[14] F. C. Larche and J. W. Cahn, *J. Res. of the National Bureau of Standards* **89**, 467 (1984).

[15] S.R. Coriell and R.L. Parker, *J. Appl. Phys.* **36**, 632 (1965).

[16] J. D. Eshelby, in *Progress in Solid Mechanics* **2**, eds. I. N. Sneddon and R. Hill, North-Holland, Amsterdam, 89 (1961).

[17] P.H. Leo and R.F. Sekerka, *Acta metall.* **37**, 3119 (1989).

[18] R.M. Christensen, *Mechanics of composite materials*, Wiley, New York (1979).

[19] J.I.D. Alexander, P.H. Leo and R.F. Sekerka, *Acta metall.* **33**, 975 (1985).

[20] Y.C. Fung, *Foundation of solid mechanics*, Prentice Hall Inc., Englewood Cliffs, New Jersey (1965).

Figure Captions

Figure 1. The progression of base shapes for $R/R^* = 2, 6, 10$ under an applied shear $\sigma_{11}^{app} = -\sigma_{22}^{app} = 0.01\mu^M$, $\sigma_{12}^{app} = 0$ and zero misfit. In all the figures, the dimensionless quantities correspond roughly to a supersaturation $(c_\infty - c_0)/(C - c_0) = 0.008$, $\mu^M = 35\,GPa$, $\gamma = 0.1\,J/m^2$ and $R^* = 10\,nm$.

Figure 2. The progression of base shapes for $R/R^* = 2, 6, 10$ under an applied shear $\sigma_{11}^{app} = -\sigma_{22}^{app} = 0.01\mu^M$, $\sigma_{12}^{app} = 0$ and zero misfit.

Figure 3. The progression of base shapes for $R/R^* = 2, 6, 10$ under an applied tension $\sigma_{11}^{app} = 0.017\mu^M$, $\sigma_{22}^{app} = \sigma_{12}^{app} = 0$ and zero misfit.

Figure 4. The progression of base shapes for $R/R^* = 2, 6, 10$ under an applied tension $\sigma_{11}^{app} = 0.017\mu^M$, $\sigma_{22}^{app} = \sigma_{12}^{app} = 0$ and zero misfit.

Figure 5. The progression of base shapes for $R/R^* = 2, 6, 10$ under an applied shear $\sigma_{11}^{app} = -\sigma_{22}^{app} = 0.009\mu^M$, $\sigma_{12}^{app} = 0$ and misfit $\epsilon^T = 0.0005$.
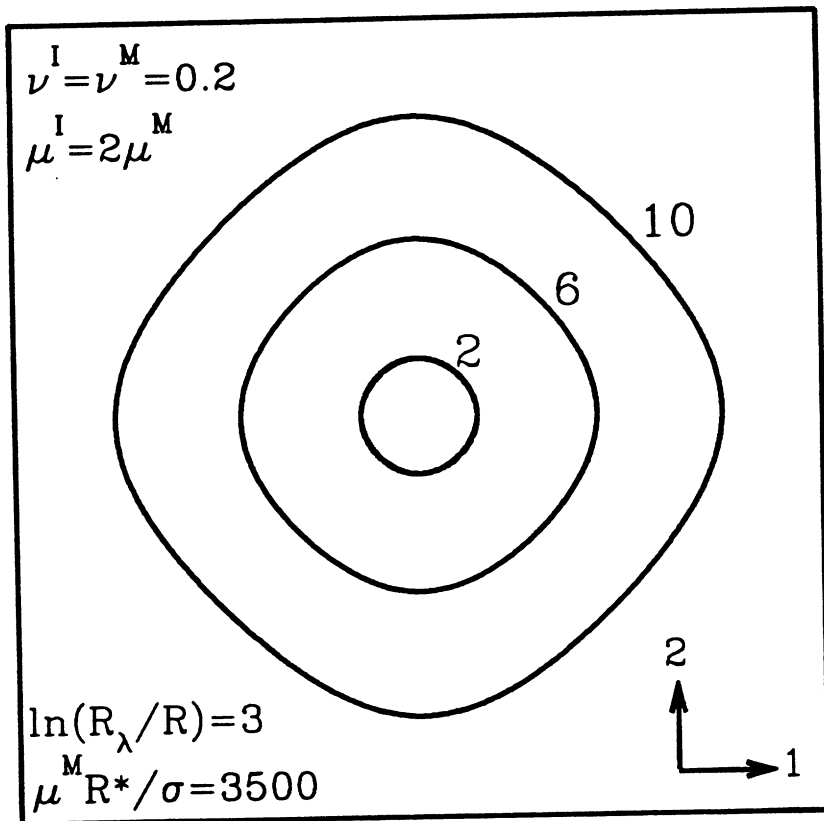
Figure 6. The progression of base shapes for $R/R^* = 2, 6, 10$ under an applied tension $\sigma_{11}^{app} = 0.017\mu^M$, $\sigma_{22}^{app} = \sigma_{12}^{app} = 0$. Figure (a) is for a misfit $\epsilon^T = -0.003$, while (b) is for $\epsilon^T = -0.006$.
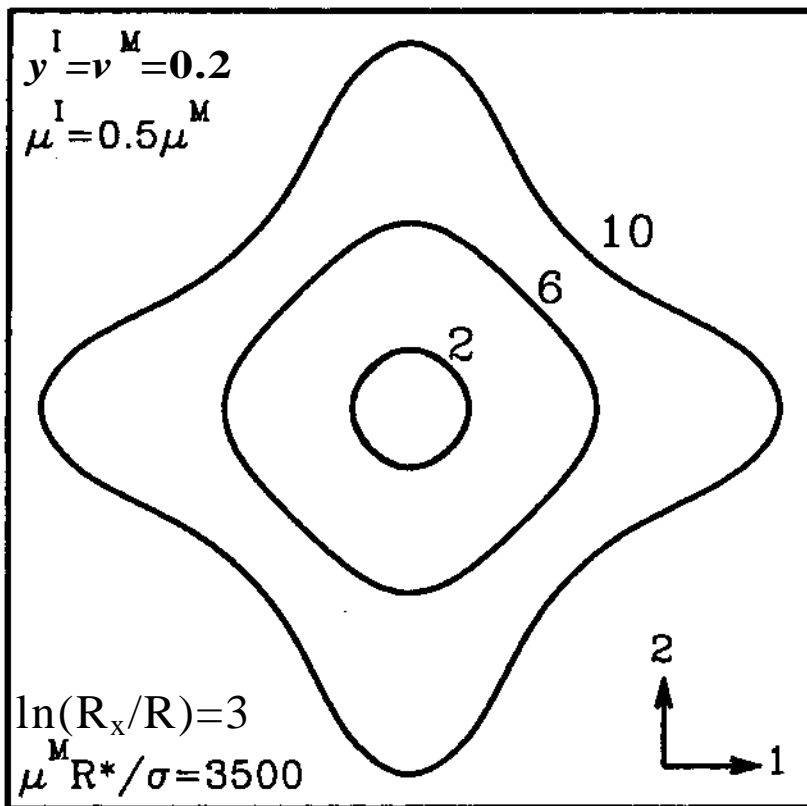
Figure 7. The critical radius $R_{cr}(3)/R^*$ as a function of $\omega = \mu^M/\mu^I$ for three misfits and an applied shear $\sigma_{11}^{app} = -\sigma_{22}^{app} = 0.005\mu^M$, $\sigma_{12}^{app} = 0$.
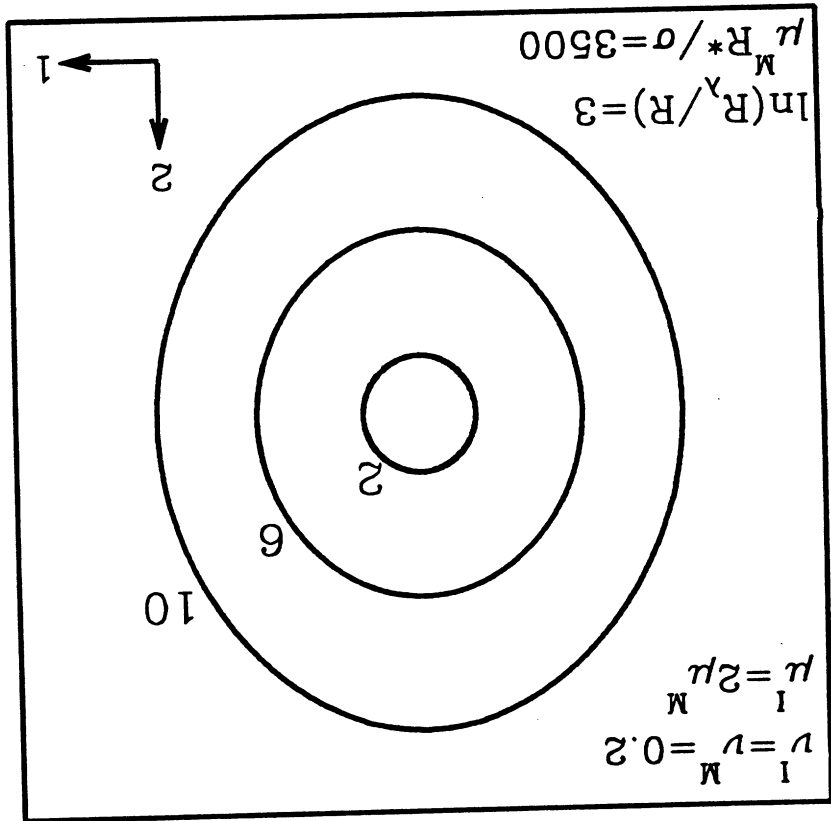
Figure 8. The critical radius $R_{cr}(3)/R^*$ as a function of $\omega = \mu^M/\mu^I$ for three misfits and an applied tension $\sigma_{11}^{app} = 0.012\mu^M$, $\sigma_{22}^{app} = \sigma_{12}^{app} = 0$.
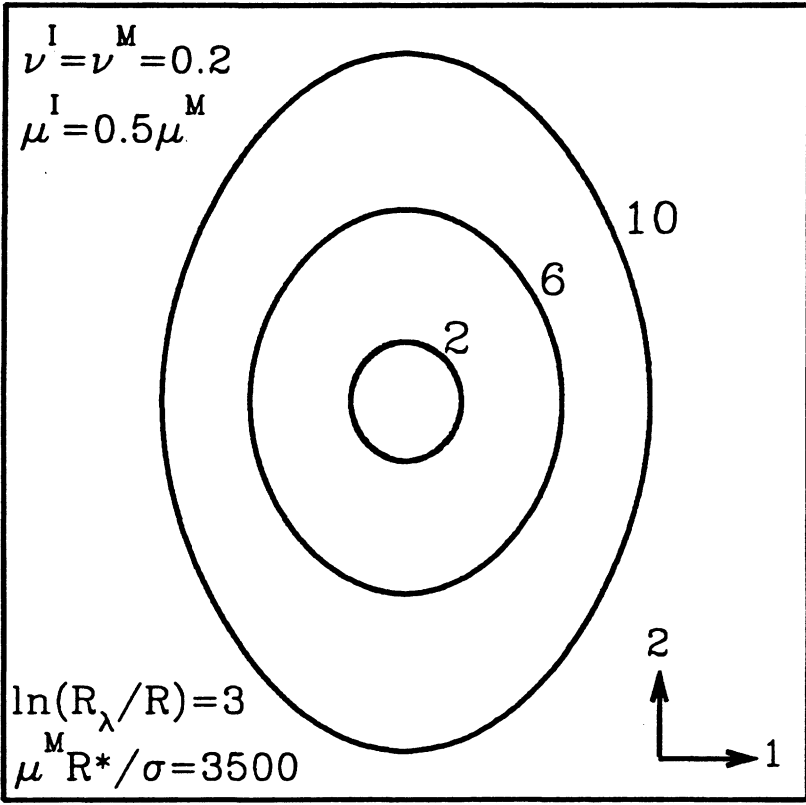
Figure 9. The critical radius $R_{cr}(3)/R^*$ as a function of $\omega = \mu^M/\mu^I$ for three values of ν^I and an applied tension $\sigma_{11}^{app} = 0.012\mu^M$, $\sigma_{22}^{app} = \sigma_{12}^{app} = 0$.
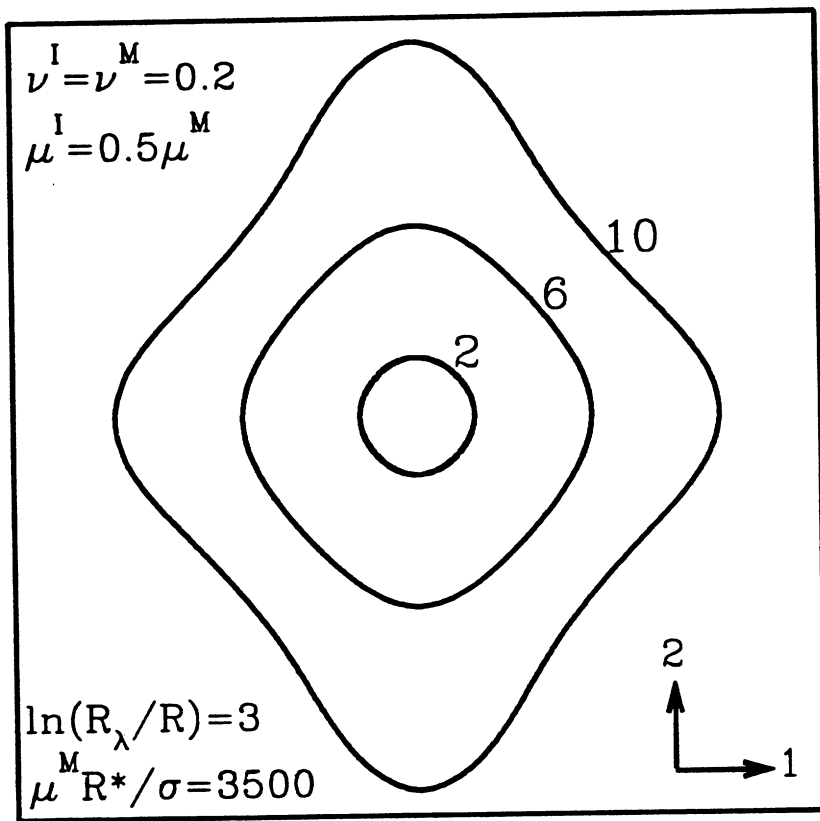
Figure 10. The critical radius $R_{cr}(3)/R^*$ as a function of the bulk modulus ratio K^M/K^I for three values of $\omega = \mu^M/\mu^I$ and an applied tension $\sigma_{11}^{app} = 0.012\mu^M$, $\sigma_{22}^{app} = \sigma_{12}^{app} = 0$.

$\nu^I = \nu^M = 0.2$

$\mu^I = 2\mu^M$

10

6

2

$\ln(R_\lambda/R) = 3$

$\mu^M R^*/\sigma = 3500$

2

1

$y^I = v^M = 0.2$

$\mu^I = 0.5\mu^M$

10

6

2

$\ln(R_x/R) = 3$

$\mu^M R^*/\sigma = 3500$

2

1

$\nu^I = \nu^M = 0.2$

$\mu^I = 0.5\mu^M$

10

6

2

$\ln(R_\lambda/R) = 3$

$\mu^M R^*/\sigma = 3500$

2

1

$\nu^I = \nu^M = 0.2$

$\mu^I = 0.5\mu^M$

10

6

2

$\ln(R_\lambda/R) = 3$

$\mu^M R^*/\sigma = 3500$

2

1

$\nu^I = \nu^M = 0.2$

$\mu^I = 0.5\mu^M$

10

6

2

$\ln(R_\lambda/R) = 3$

$\mu^M R^*/\sigma = 3500$

2

1

Plot of $R_{cr}(3)/R^*$ versus ω with labeled curves $\epsilon^T=0$, $\epsilon^T=-0.1\%$, and $\epsilon^T=+0.1\%$. Parameters: $\mu^M R^*/\sigma=3500$, $\ln(R_\lambda/R)=3$, $\nu^I=\nu^M=0.2$.

Axis labels and annotations:

$R_{cr}(3)/R^*$ (vertical axis)

75

70

65

$\nu^I = 0.4$

$\nu^I = 0.2$

$\nu^I = 0.3$

$\nu^M = 0.3$
$\ln(R_\lambda/R) = 3$
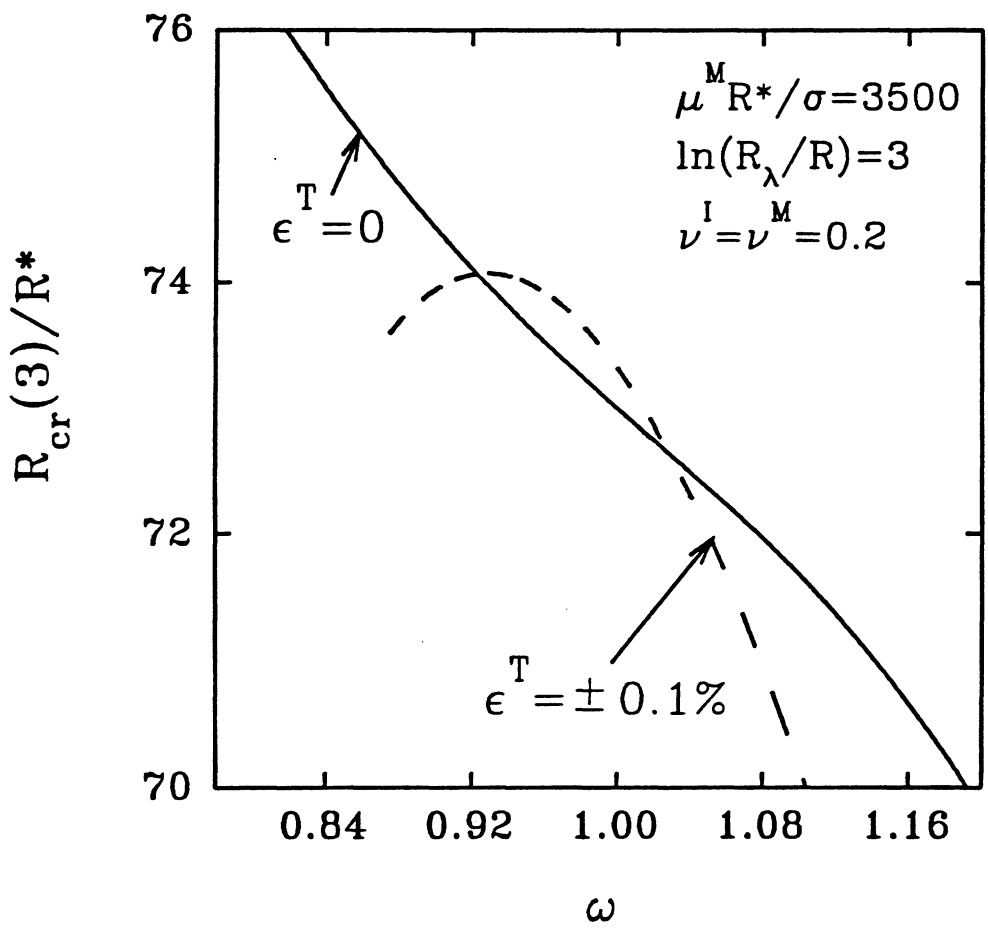$\mu^M R^*/\sigma = 3500$
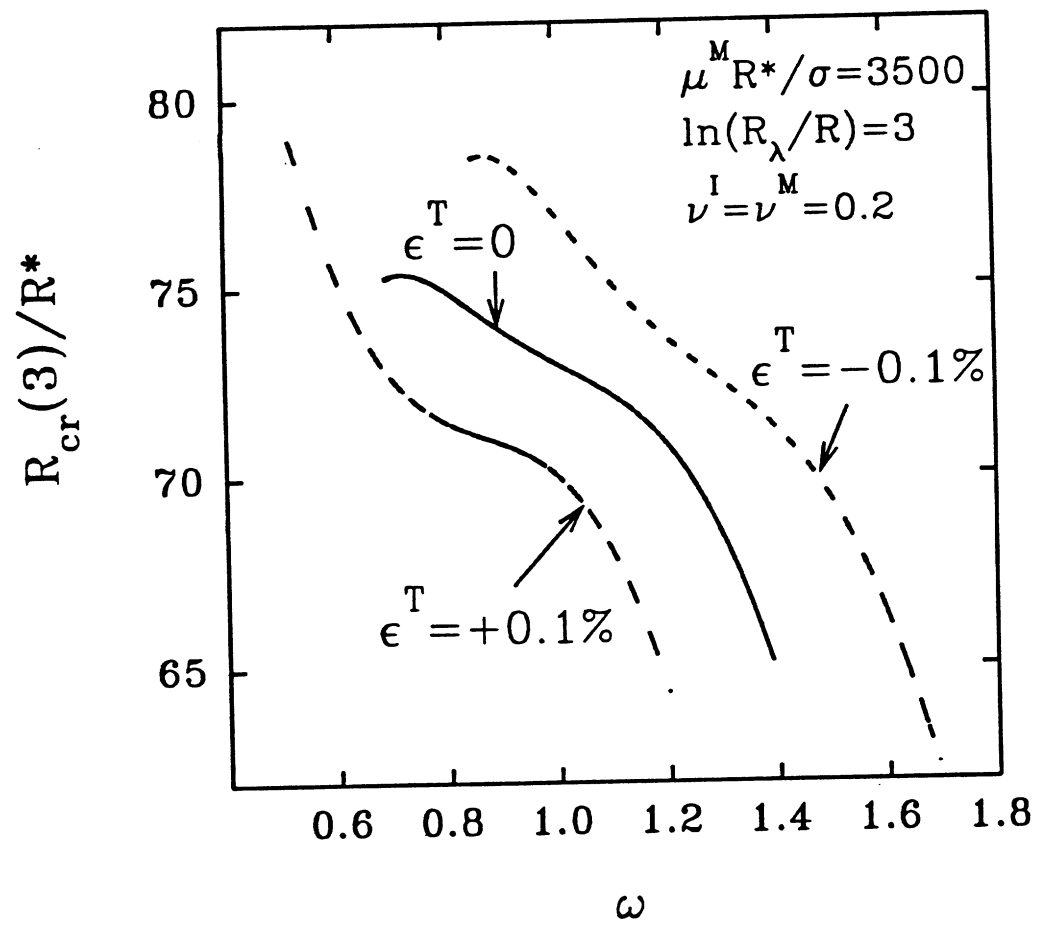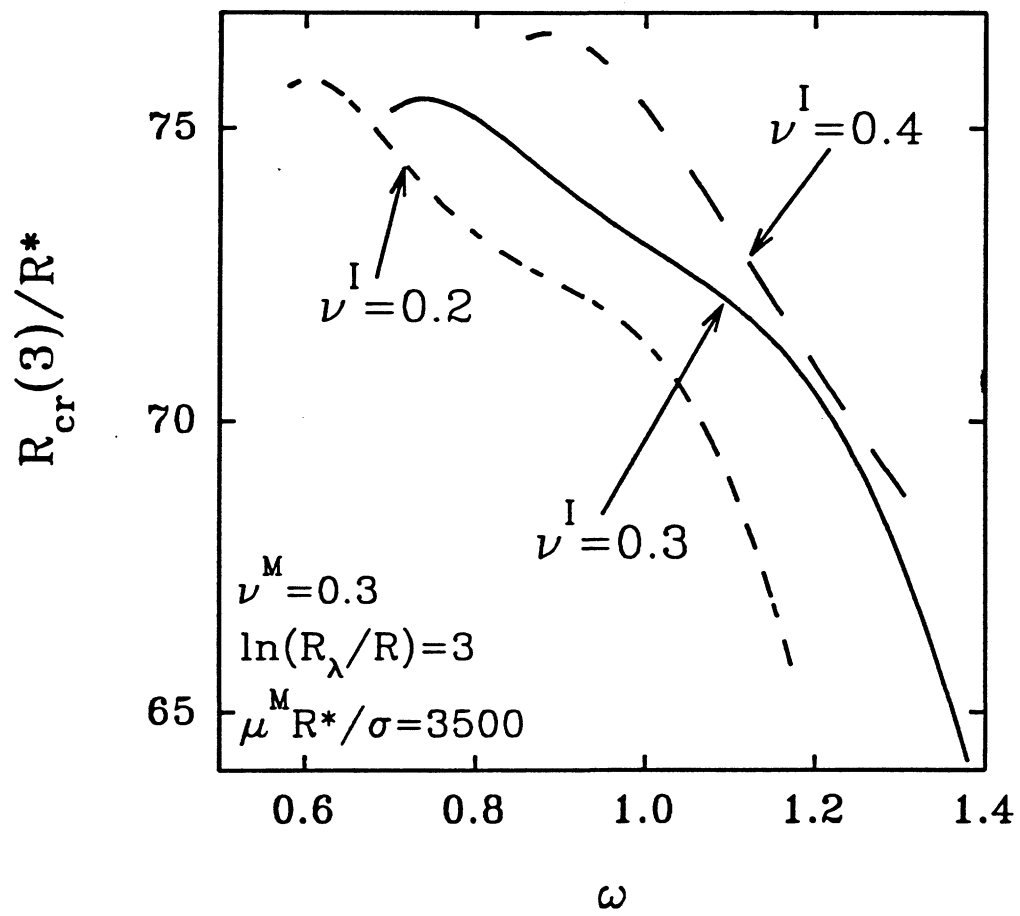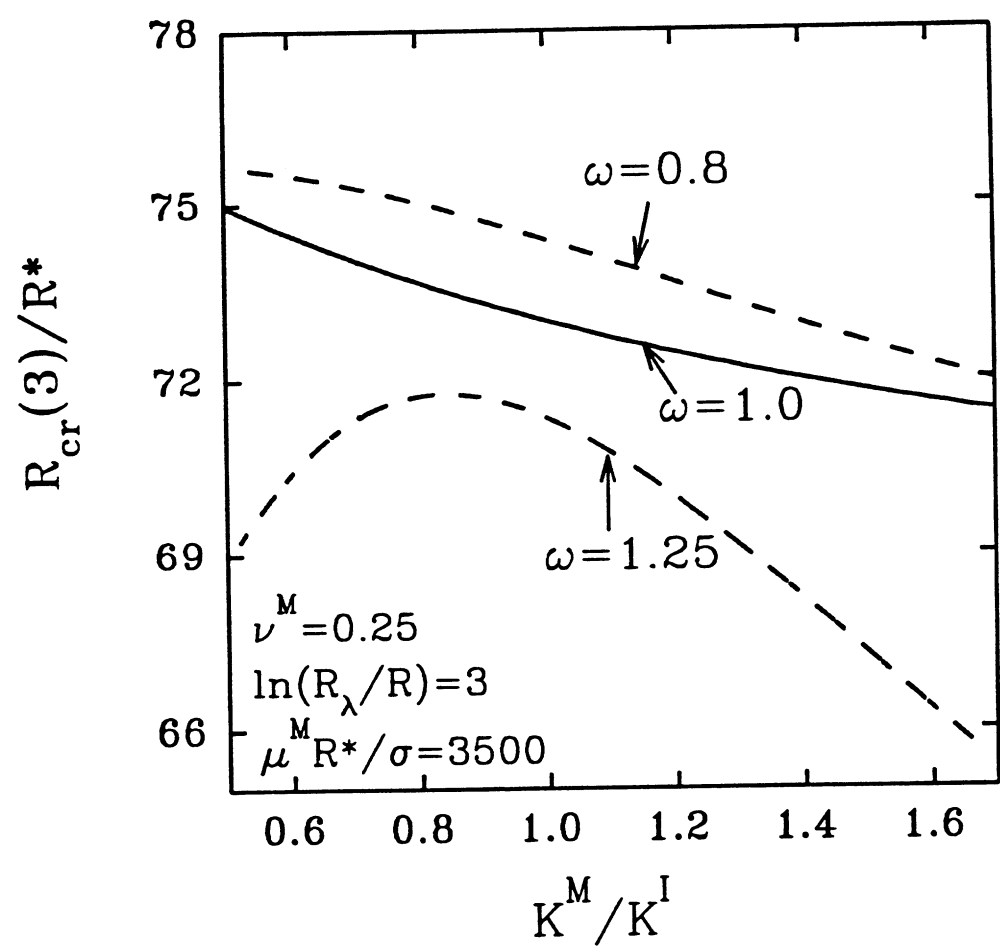
0.6   0.8   1.0   1.2   1.4

ω
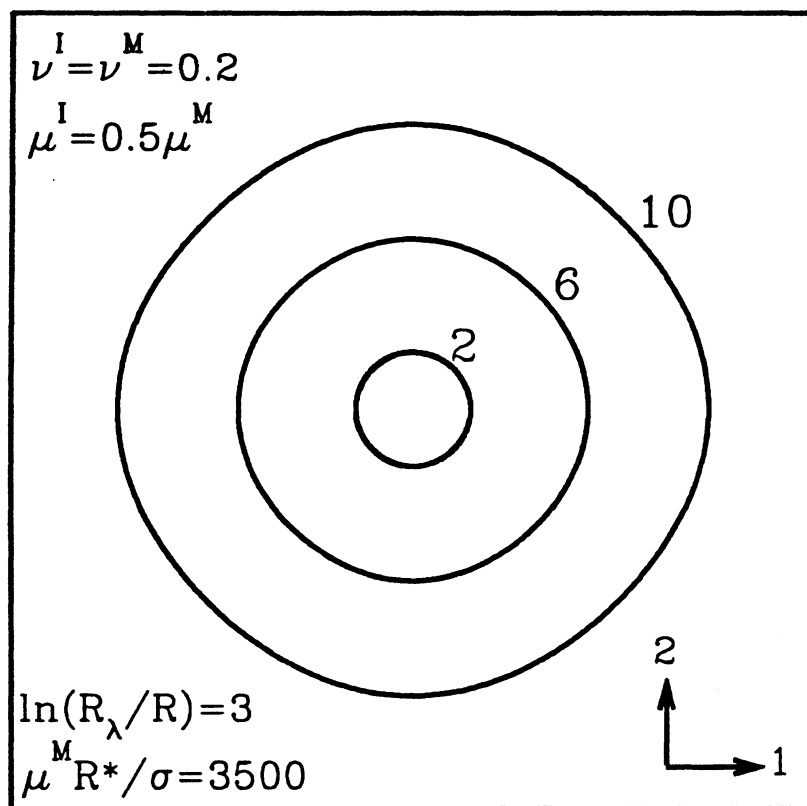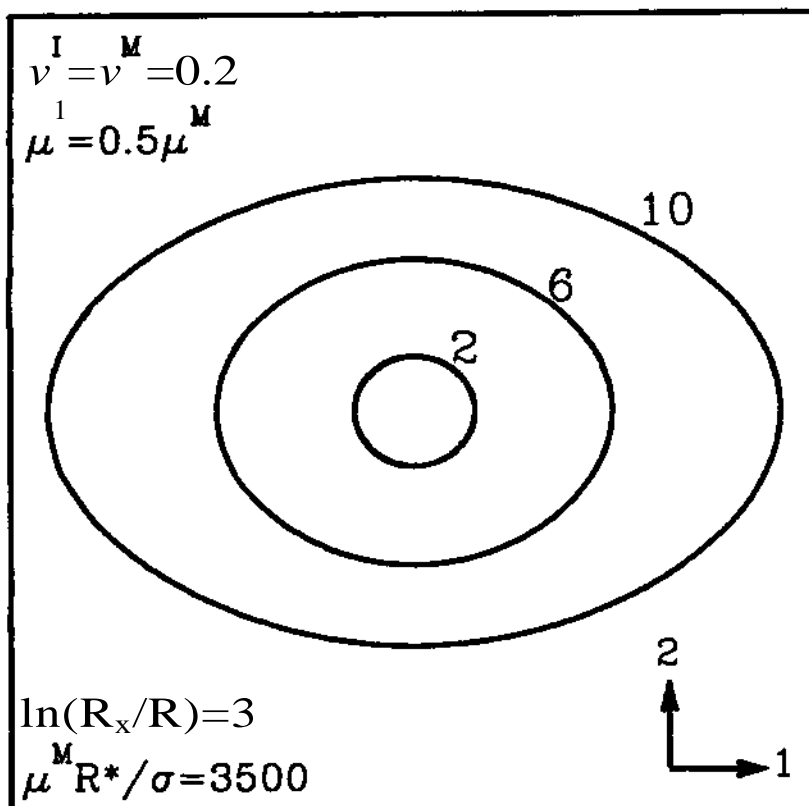
Center for Nonlinear Analysis
Report Series • Complete List

Nonlinear Analysis Series

No.

91-NA-001   [ ]   Lions, P.L., **Jacobians and Hardy spaces**, June 1991

91-NA-002   [ ]   Giga, Y. and Soto, M.-H., **Generalized interface evolution with the Neumann boundary condition**, July 1991

91-NA-003   [ ]   Soner, H.M. and Souganidis, P.E., **Uniqueness and singularities of cylindrically symmetric surfaces moving by mean curvature**, July 1991

91-NA-004   [ ]   Coleman, B.D., Marcus, M. and Mizel, V.J., **On the Thermodynamics of periodic phases**, August 1991

91-NA-005   [ ]   Gurtin, M.E. and Podio-Guidugli, P., **On the formulation of mechanical balance laws for structured continua**, August 1991

91-NA-006   [ ]   Gurtin, M.E. and Voorhees, P., **Two-phase continuum mechanics with mass transport and stress**, August 1991

91-NA-007   [ ]   Fried, E., **Non-monotonic transformation kinetics and the morphological stability of phase boundaries in thermoelastic materials**, September 1991

91-NA-008   [ ]   Gurtin, M.E., **Evolving phase boundaries in deformable continua**, September 1991

91-NA-009   [ ]   Di Carlo, A., Gurtin, M.E., and Podio-Guidugli, P., **A regularized equation for anisotropic motion-by-curvature**, September 1991

91-NA-010   [ ]   Kinderlehrer, D. and Ou, B., **Second variation of liquid crystal energy at $x/|x|$**, August 1991

91-NA-011   [ ]   Baughman, L.A. and Walkington, N., **Co-volume methods for degenerate parabolic problems**, August 1991

91-NA-012   [ ]   James, R.D. and Kinderlehrer, D., **Frustration and microstructure: An example in magnetostriction**, November 1991

91-NA-013   [ ]   Angenent, S.B. and Gurtin, M.E., **Anisotropic motion of a phase interface**, November 1991

92-NA-001 [ ] Nicolaides, R.A. and Walkington, N.J., **Computation of microstructure utilizing Young measure representations,** January 1992

92-NA-002 [ ] Tartar, L., **On mathematical tools for studying partial differential equations of continuum physics: H-measures and Young measures,** January 1992

92-NA-003 [ ] Bronsard, L. and Hilhorst, D., **On the slow dynamics for the Cahn-Hilliard equation in one space dimension,** February 1992

92-NA-004 [ ] Gurtin, M.E., **Thermodynamics and the supercritical Stefan equations with nucleations,** March 1992

92-NA-005 [ ] Antonic, N., **Memory effects in homogenisation linear second order equation,** February 1992

92-NA-006 [ ] Gurtin, M.E. and Voorhees, **P.W., The continuum mechanics of coherent two-phase elastic solids with mass transport,** March 1992

92-NA-007 [ ] Kinderlehrer, D. and Pedregal, **P., Remarks about gradient Young measures generated by sequences in Sobolev spaces,** March 1992

92-NA-008 [ ] **Workshop on Shear Bands,** March 23-25,1992 (Abstracts), March 1992

92-NA-009 [ ] Armstrong, **R.** W., **Microstructural/Dislocation Mechanics Aspects of Shear Banding in Polycrystals,** March 1992

92-NA-010 [ ] Soner, H. M. and Souganidis, **P.** E., **Singularities and Uniqueness of Cylindrically Symmetric Surfaces Moving by Mean Curvature,** April 1992

92-NA-011 [ ] Owen, David R., Schaeffer, Jack, and Wang, Keming, **A Gronwall Inequality for Weakly Lipschitzian Mappings,** April 1992

92-NA-012 [ ] Alama, Stanley and Li, **Yan Yan, On "Multibump" Bound States for Certain Semilinear Elliptic Equations,** April 1992

92-NA-013 [ ] Olmstead, W. E., Nemat-Nasser, S., and Li, **L., Shear Bands as Discontinuities, April** 1992

92-NA-014 [ ] **Antonic, N., H-Measures Applied to Symmetric Systems,** April 1992

92-NA-015 [ ] Barroso, Ana Cristina and Fonseca, Irene, **Anisotropic Singular Perturbations • The Vectorial Case,** April 1992

92-NA-016 [ ] Pedregal, Pablo, **Jensen's Inequality in the Calculus of Variations,** May 1992

92-NA-017 [ ] Fonseca, Irene and Muller, Stefan, **Relaxation of Quasiconvex Functional in BV(ft,SRP) for Integrands f(x,u,Vu),** May 1992

92-NA-018   [ ]   Alama, Stanley and Tarantello, Gabriella, **On Semilinear Elliptic Equations with Indefinite Nonlinearities**, May 1992

92-NA-019   [ ]   Owen, David R., **Deformations and Stresses With and Without Microslip**, June 1992

92-NA-020   [ ]   Barles, G., Soner, H. M., Souganidis, P. E., **Front Propagation and Phase Field Theory**, June 1992

92-NA-021   [ ]   Bruno, Oscar P. and Reitich, Fernando, **Approximation of Analytic Functions: A Method of Enhanced Convergence**, July 1992

92-NA-022   [ ]   Bronsard, Lia and Reitich, Fernando, **On Three-Phase Boundary Motion and the Singular Limit of a Vector-Valued Ginzburg-Landau Equation**, July 1992

92-NA-023   [ ]   Cannarsa, Piermarco, Gozzi, Fausto and Soner, H.M., **A Dynamic Programming Approach to Nonlinear Boundary Control Problems of Parabolic Type**, July 1992

92-NA-024   [ ]   Fried, Eliot and Gurtin, Morton, **Continuum Phase Transitions With An Order Parameter; Accretion and Heat Conduction**, August 1992

92-NA-025   [ ]   Swart, Pieter J. and Homes, Philip J., **Energy Minimization and the Formation of Microstructure in Dynamic Anti-Plane Shear**, August 1992

92-NA-026   [ ]   Ambrosio, I., Cannarsa, P. and Soner, H.M., **On the Propagation of Singularities of Semi-Convex Functions**, August 1992

92-NA-027   [ ]   Nicolaides, R.A. and Walkington, Noel J., **Strong Convergence of Numerical Solutions to Degenerate Varational Problems**, August 1992

92-NA-028   [ ]   Tarantello, Gabriella, **Multiplicity Results for an Inhomogenous Neumann Problem with Critical Exponent**, August 1992

92-NA-029   [ ]   Noll, Walter, **The Geometry of Contact, Separation, and Reformation of Continous Bodies**, August 1992

92-NA-030   [ ]   Brandon, Deborah and Rogers, Robert C., **Nonlocal Superconductivity**, July 1992

92-NA-031   [ ]   Yang, Yisong, **An Equivalence Theorem for String Solutions of the Einstein-Matter-Gauge Equations**, September 1992

92-NA-032   [ ]   Spruck, Joel and Yang,Yisong, **Cosmic String Solutions of the Einstein-Matter-Gauge Equations**, September 1992

92-NA-033   [ ]   **Workshop on Computational Methods in Materials Science (Abstracts)**, September 16-18, 1992.
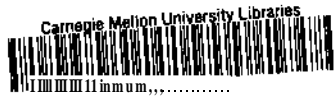
92-NA-034   [ ]   Leo, Perry H. and Herng-Jeng Jou, **Shape evolution of an initially circular precipitate growing by diffusion in an applied stress field**, October 1992

92-NA-035   [ ]   Gangbo, Wilfrid, **On the weak lower semicontinuity of energies with polyconvex integrands**, October 1992

92-NA-036   [ ]   Katsoulakis, Markos, Kossioris, Georgios T. and Retich, Fernando, **Generalized motion by mean curvature with Neumann conditions and the Allen-Cahn model for phase transitions**, October 1992

92-NA-037   [ ]   Kinderlehrer, David, **Some methods of analysis in the study of microstructure**, October 1992

92-NA-038   [ ]   Yang, Yisong, **Self duality of the Gauge Field equations and the Cosmological Constant**, November 1992

92-NA-039   [ ]   Brandon, Deborah and Rogers, Robert, **Constitutive Laws for Pseudo-Elastic Materials**, November 1992

92-NA-040   [ ]   Leo, P. H., Shield, T. W., and Bruno, O. P., **Transient Heat Transfer Effects on the Pseudoelastic Behavior of Shape-Memory Wires**, November 1992

92-NA-041   [ ]   Gurtin, Morton E., **The Dynamics of Solid-Solid Phase Transitions 1. Coherent Interfaces**, November 1992

92-NA-042   [ ]   Gurtin, Morton E., Soner, H. M., and Souganidis, P. E., **Anisotropic Motion of an Interface Relaxed by the Formation of Infinitesimal Wrinkles**, December 1992

92-NA-043   [ ]   Bruno, Oscar P., and Fernando Reitich, **Numerical Solution of Diffraction Problems: A Method of Variation of Boundaries II. Dielectric gratings, Padé Approximants and Singularities**, December 1992

93-NA-001   [ ]   Mizel, Victor J., **On Distribution Functions of the Derivatives of Weakly Differentiable Mappings**, January 1993

93-NA-002   [ ]   Kinderlehrer, David, Ou, Biao and Walkington, Noel, **The Elementary Defects of the Oseen-Frank Energy for a Liquid Crystal**, January 1993

93-NA-003   [ ]   Bruno, Oscar P., Reitich, Fernando, **Numerical Solutions of Diffraction Problems: A Method of Variation of Boundaries III. Doubly Periodic Gratings**, January 1993

93-NA-004   [ ]   James, Richard and Kinderlehrer, David, **Theory of Magnetostriction with Applications to $Tb_xDy_{1-x}Fe_2$**, February 1993

93-NA-005   [ ]   Del Piero, Gianpietro and Owen, David R., **Structured Deformations of Continua**, February 1993

93-NA-006   [ ]   Cheng, Chih-Wen and Mizel, Victor J., **On the Lavrentiev Phenomenon for Autonomous Second Order Integrands**, February 1993

93-NA-007   [ ]   Ma, Ling, **Computation of Magnetostrictive Materials**, February 1993

93-NA-008   [ ]   James, Richard and Kinderlehrer, David, **Mathematical Approaches to the Study of Smart Materials**, February 1993

93-NA-009   [ ]   Kinderlehrer, David, Nicolaides, Roy, and Wang, Han, **Spurious Oscillations in Computing Microstructures,** February 1993

93-NA-010   [ ]   Ma, Ling and Walkington, Noel, **On Algorithms for Non-Convex Optimization,** February 1993

93-NA-011   [ ]   Fonseca, Irene, Kinderlehrer, David, and Pedregal, Pablo, **Relaxation in BV x L^{∞} of Functionals Depending on Strain and Composition,** February 1993

93-NA-012   [ ]   Izumiya, Shyuichi and Kossioris, Georgios T., **Semi-Local Classification of Geometric Singularities for Hamilton-Jacobi Equations,** March 1993

93-NA-013   [ ]   Du, Qiang, **Finite Element Methods for the Time-Dependent Ginzburg-Landau Model of Superconductivity,** March 1993

Stochastic Analysis Series

91-SA-001   [ ]   Soner, H.M., **Singular perturbations in manufacturing,** November 1991

91-SA-002   [ ]   Bridge, D.S. and Shreve, S.E., **Multi-dimensional finite-fuel singular stochastic control,** November 1991

92-SA-001   [ ]   Shreve, S. E. and Soner, H. M., **Optimal Investment and Consumption with Transaction Costs,** September 1992